

Cite this: *Nanoscale*, 2011, **3**, 2903

www.rsc.org/nanoscale

PAPER

Large area flexible SERS active substrates using engineered nanostructures†

Aram J. Chung,^a Yun Suk Huh^{ab} and David Erickson^{*a}

Received 11th March 2011, Accepted 29th April 2011

DOI: 10.1039/c1nr10265f

Surface enhanced Raman scattering (SERS) is an analytical sensing method that provides label-free detection, molecularly specific information, and extremely high sensitivity. The Raman enhancement that makes this method attractive is mainly attributed to the local amplification of the incident electromagnetic field that occurs when a surface plasmon mode is excited at a metallic nanostructure. Here, we present a simple, cost effective method for creating flexible, large area SERS-active substrates using a new technique we call shadow mask assisted evaporation (SMAE). The advantage of large, flexible SERS substrates such as these is they have more area for multiplexing and can be incorporated into irregular surfaces such as clothing. We demonstrate the formation of four different types of nanostructure arrays (pillar, nib, ellipsoidal cylinder, and triangular tip) by controlling the evaporation angle, substrate rotation, and deposition rate of metals onto anodized alumina nanoporous membranes as large as 27 mm. In addition, we present experimental results showing how a hybrid structure comprising of gold nanospheres embedded in a silver nano-pillar structure can be used to obtain a 50× SERS enhancement over the raw nanoparticles themselves.

Introduction

The high sensitivity and potential for label-free analysis associated with surface enhanced Raman scattering (SERS) has made it an attractive analytical technique for applications ranging from DNA sequencing to pathogen identification.^{1–6} To obtain reproducible SERS enhancement over large areas^{7–12} several nanofabrication methods (*e.g.* electron beam lithography,^{13–17} focused ion-beam lithography,¹⁸ and nano-transfer printing^{19,20}) have been used to create nanostructured arrays with precisely controlled shapes and sizes.²¹ Achieving uniformity of the nanostructures over large scales is important since the Raman signal intensity is extremely sensitive to the size, shape, and morphology of the structures on the substrate.²² These techniques provide extremely uniform signal enhancement but are complex, expensive, and have very low-throughput.

To address this, numerous methods have been developed to create substrates with the same level of uniformity but with much less reliance on traditional nanofabrication technologies.^{23–25} Some of the more prominent examples include: nanosphere lithography (NSL),^{26,27} metal film over nanosphere (MFON),^{8,28,29} and shadow overlap of ion-beam lithography (SOISL).³⁰ Most of these

alternatives utilize self-assembled nanospheres to create uniform morphologies on top of a base substrate which can serve as a mask during a metal evaporation process. Alternative approaches such as the direct use of self-assembled metallic nanostructures^{5,31,32} have also been demonstrated. The spatial range over which uniformity can be achieved with these techniques is limited by the size of the crystalline structure obtained during the self-assembly process.

In this paper, we present a new high throughput method for creating uniform, large area, and flexible SERS-active substrates. Flexible and large area SERS substrates are useful because they can be more easily incorporated into irregularly shaped surfaces such as clothing, and have greater spatial area for multiplexing. We refer to our technique as shadow mask assisted evaporation (SMAE). Previously, we reported the creation of nanotubular structures fabricated using a similar method and applied them to the aptamer based detection of vasopressin.³³ We expand significantly on the technique here and explore how the various evaporation conditions such as incident angle, substrate rotation, and deposition rate allow us to create a wide range of controllable 3D SERS-active nanostructures. We describe the fabrication technique and characterize how the above parameters affect the topography of the structures that are created. Characterization of the resulting SERS enhancement factor is done using experimental techniques and the optimal structures are applied to the detection of short nucleic acid sequences.

Results and discussion

Nanostructure fabrication

Fig. 1a shows a schematic of the SMAE process. Briefly, metal (Ag or Au) is deposited on an anodized aluminium oxide

^aSibley School of Mechanical and Aerospace Engineering, Cornell University, Ithaca, NY, 14853, USA. E-mail: de54@cornell.edu; Fax: +1 607-255-1222; Tel: +1 607-255-4861

^bDivision of Materials Science, Korea Basic Science Institute, Daejeon, 305-333, Korea. E-mail: yshuh@kbsi.re.kr

† Electronic supplementary information (ESI) available: Two figures showing an angle dependence of the nanostructure formation and uniformity of four types of SERS-active substrates. See DOI: 10.1039/c1nr10265f

(AAO) nanoporous template at an angle, α , such that the inner walls and top can be coated. Following evaporation the AAO template is dissolved in a NaOH solution and the metallic nanostructure film is allowed to settle onto the top of a poly(dimethylsiloxane) (PDMS) substrate (further fabrication details are available in the Materials and methods section). Using this technique we are able to construct nanostructure arrays as large as 27 mm in diameter limited only by the size of the template. Some other alternative methods^{30,31} reported larger substrates however the SMAE has numerous advantages including the simplicity in fabrication, the cost, the flexibility, and the relative large area. Fig. 1b shows the SEM images of Ag “nano-pillar” structures obtained using a 45° incident angle, and evaporation rates of (1) 0.8 Å s⁻¹ and (2) 1.2 Å s⁻¹. The tip of the nano-pillar structure shown in Fig. 1b(1) (445 ± 55 nm; single structure height ± standard deviation) is much sharper than that shown in Fig. 1b(2) (340 ± 45 nm) suggesting that higher evaporation rates yield coarser structures. As shown in Fig. 1b(3) and (4), the placement of the nanostructure film on the PDMS support enables these substrates to be robust and still highly flexible. In addition to the advantages described above, this flexibility also allows the spacing of the nano-pillars to be modified by mechanical stress which could be useful for tuning the optical response.

In order to determine the dependence of the incident angle of evaporation, α , on the resulting structure of the nano-pillars, experiments were also performed for $\alpha = 30^\circ$ and 60° , the results of which can be seen in Fig. S1 in the ESI†. The 30° case yielded the sharpest nanostructures however during the dissolution of the AAO membrane the relatively tall and weak pillars tended to collapse (see Fig. S1a and b†). For a 60° incident angle, shadowing resulted in shorter and less sharp nano-pillars (see Fig. S1c and d†) than what was observed for the 45° case. Stronger fields are normally achieved from sharper morphologies.^{34–36} Based on the above results, evaporation conditions at an incident angle of 45° and a deposition rate of 0.8 Å s⁻¹ were chosen as the optimal conditions and used for the rest of this study.

To further explore this approach, we fabricated three additional types of nanostructure arrays. Fig. 2b illustrates the “nano-nib” shape (type II) structures obtained through double evaporation. To fabricate this structure, 100 nm of silver was first deposited with a 45° incident angle. An additional 100 nm of silver was then deposited with $\alpha = 45^\circ$ and a substrate rotation speed of 35 rpm. We observed arrays of structures 405 ± 57 nm in height with 173 ± 25 nm hole diameters (as defined in Fig. 1a). In another approach, the “nano-ellipsoidal cylinder” structure (type III, Fig. 2c) was constructed using the same conditions except that the substrate was rotated during the initial metal

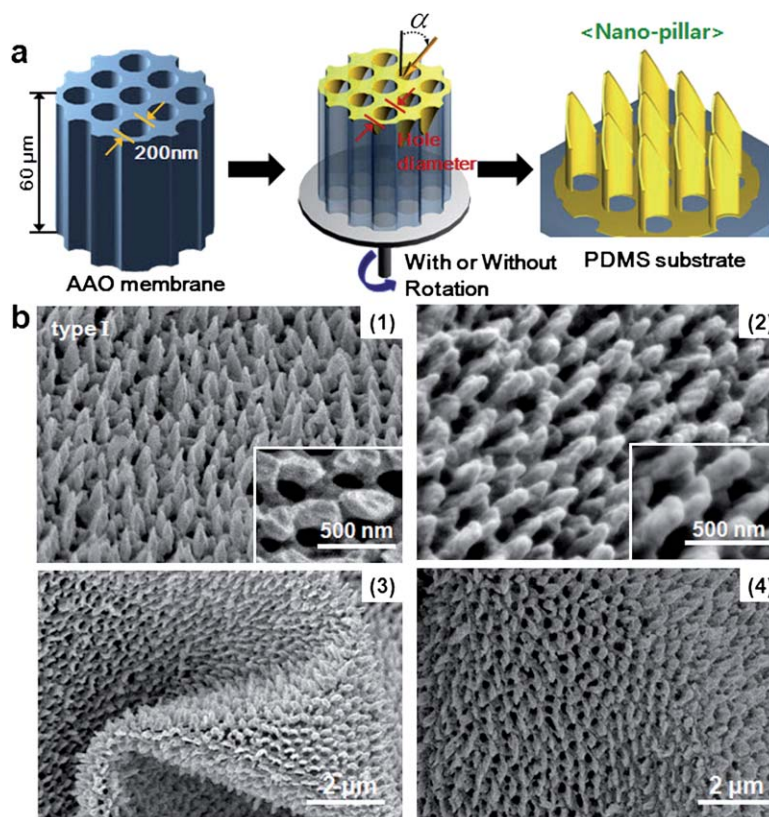


Fig. 1 SERS-active nanostructure arrays fabricated by shadow mask assisted evaporation (SMAE). (a) Schematic showing the stages of fabrication for the nano-pillar arrays (not to scale). After attaching an anodic alumina oxide membrane onto a silicon substrate, the desired metal structure is coated onto the membrane by changing the incident angle (α) and rotation condition. The AAO membrane is dissolved with NaOH, and the metallic nanostructure arrays are transferred to a poly(dimethylsiloxane) substrate. (b) SEM images of the Ag “nano-pillar” structures obtained using $\alpha = 45^\circ$ and evaporation rates of (1) 0.8 Å s⁻¹ and (2) 1.2 Å s⁻¹. No rotation was applied. (3 and 4) Images demonstrating the flexibility of the nanostructure film.

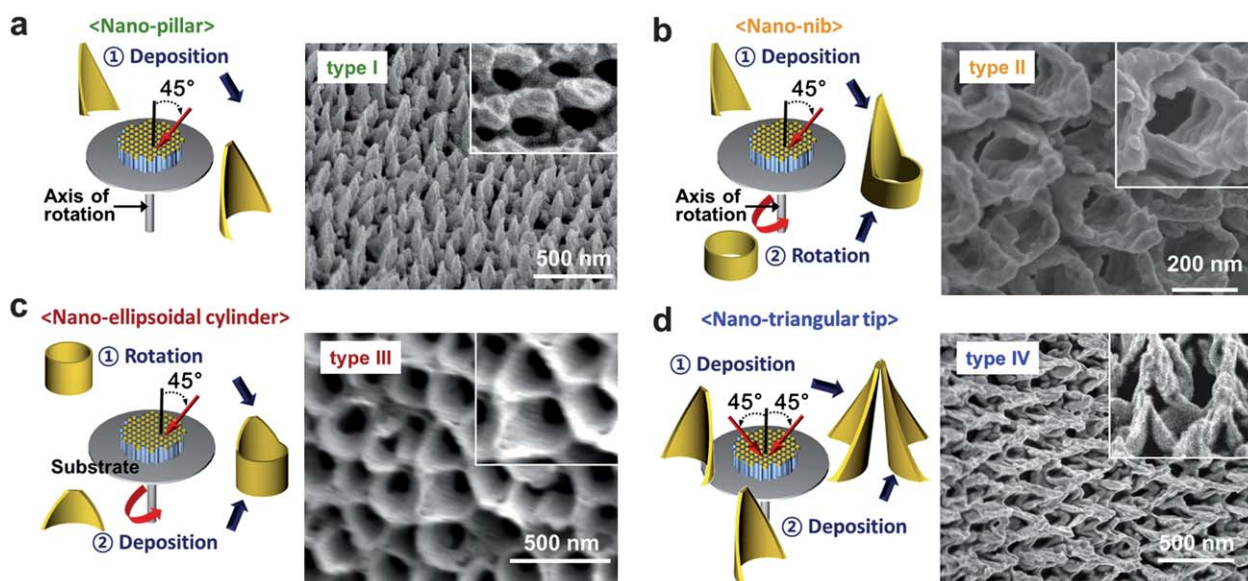


Fig. 2 Fabrication of type I, II, III and IV SERS-active nanostructures. (a) Type I nano-pillar structures created with a single metal deposition step using an incident angle of 45° . (b) Type II nano-nib structures produced by a two-step evaporation process: first 100 nm of metal is deposited at an incident angle of 45° , followed by an additional 100 nm deposition at a 45° angle while rotating the substrate at 35 rpm. (c) Type III nano-ellipsoidal cylindrical structures also formed in a two-step process, first by depositing 100 nm of metal at a 45° angle while rotating the substrate at 35 rpm, then depositing another 100 nm of metal also at a 45° angle without rotating the substrate. (d) Type IV nano-triangular tip structures were fabricated by double depositions from 45° and 135° angles of incidence. See Table 1 for detailed conditions and specifications.

deposition and then not rotated for the second silver evaporation step. 320 ± 35 nm and 165 ± 21 nm were measured for height and hole diameter respectively. The fourth type of nanostructures were obtained by depositing silver twice with $\alpha = 45^\circ$ and 135° . The resulting “nano-triangular tip” structure (type IV) shown in Fig. 2d had a height of 220 ± 24 nm and a hole diameter of 175 ± 27 nm. Table 1 summarizes the fabrication conditions and specifications for all nanostructures developed here. Although only small portion of the entire substrate can be imaged (wider view SEM images are shown in Fig. S2 in the ESI†), all nanostructure arrays exhibited high periodicity and uniformity. Various hole sizes can be obtained using different AAO templates (membranes with nanopores ranging from 20 to 200 nm in diameter are commercially available).

Raman characterization

Raman signatures were obtained to characterize the relative sensitivity of each nanostructure array developed here. As our

detection target, we used TAMRA-labeled nucleic acid sequences analogous to Dengue virus serotype 2 (DENV-2a). Details on the sample preparation techniques used here and this target are available from our previous paper³⁷ and in the Materials and methods section. To facilitate biocompatibility, prior to conducting the experiments each silver nanostructure was coated with 5 nm of gold.³³ Fig. 3 shows the SERS spectra obtained from the four different SERS-active substrates. In all cases, a solution containing 300 nM of the target DNA was pipetted onto the surface. Negative controls were not conducted here as the goal of this experiment was to measure the relative sensitivity of the surfaces using a common sample rather than conduct a formal detection reaction. Details of the Raman measurements are included in the Materials and methods section. As expected characteristic Raman peaks for the TAMRA-labeled DNA were found at 1640 , 1573 , 1482 , 1385 , and 1217 cm^{-1} . The difference in Raman intensity at 1385 cm^{-1} was used for relative sensitivity evaluation. We found the nano-triangular tip (type IV) and nano-ellipsoidal cylinder (type III) to be the most and least

Table 1 Specifications and fabrication conditions for all fabricated nanostructure arrays

| Parameters/type | Nano-pillar (type I) | Nano-nib (type II) | Nano-ellipsoidal cylinder (type III) | Nano-triangular tip (type IV) |
|----------------------------------|----------------------|--------------------|--------------------------------------|-------------------------------|
| Height/nm | 445 ± 55 | 405 ± 57 | 320 ± 35 | 220 ± 24 |
| Hole diameter/nm | 178 ± 20 | 173 ± 25 | 165 ± 21 | 175 ± 27 |
| Deposition thickness/nm | 200 | 100/100 | 100/100 | 100/100 |
| Angle/degree | 45° | $45^\circ/0^\circ$ | $0^\circ/45^\circ$ | $45^\circ/135^\circ$ |
| Rotation | No | No/yes | Yes/no | No/no |
| Relative sensitivity (\pm SD) | 1.94 ± 0.12 | 1.82 ± 0.22 | 1 | 2.4 ± 0.35 |

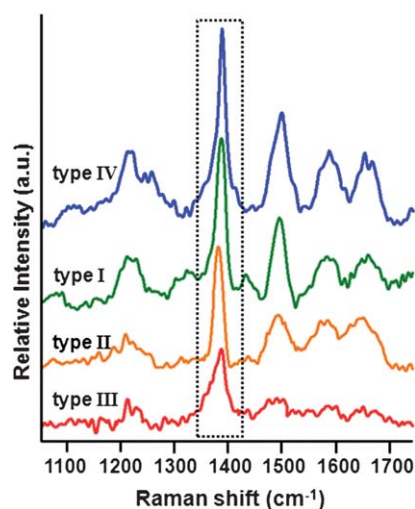


Fig. 3 SERS spectra after following immobilization of TAMRA-labeled DENV-2a for type I through type IV substrates. All measurements are conducted using a test solution initially concentrated at 300 nM. The response at 1385 cm^{-1} (dotted region) was used to compare the relative sensitivity of the substrates.

sensitive arrays respectively. Comparing the relative sensitivity of the other structures to the nano-ellipsoidal cylinder yielded enhancements of: 1.82 ± 0.22 for the nano-nib (average \pm standard deviation), 1.94 ± 0.12 for the nano-pillar, and 2.4 ± 0.35 for the nano-triangular tip structure. Although the nano-triangular tip arrays (type IV) had the greatest enhancement owing to their sharper tip morphology, the nano-pillar arrays (type I) showed the most reproducible SERS signals (smallest standard deviation). The reason for this greater reproducibility is likely because the type I structures are made using a single step fabrication process (as opposed to the type IV which uses a double step process).

Integration of nanostructured substrates with Au nanoparticles

The Raman signals from our nanostructured surfaces can be further enhanced by integrating them with Au nanoparticles. We demonstrate this here with the nano-pillar array (type I) substrates as it exhibited the greatest reproducibility. Fig. 4a and b schematically show how the nanoparticles settle into the nanostructures. The close interaction between the pillars and the nanoparticles causes a coupling of the plasmonic resonances leading to a localized hot spot as has been demonstrated by others.^{38–40} As shown in the figure TAMRA-labeled DENV-2a was attached to the Au nanospheres not the Ag SERS-active substrate. Fig. 4b shows the resulting SERS spectra from the: (1) 200 nm Au nanoparticles after settling on the surface (2) Ag nano-pillar substrate without nanoparticles (similar to the type I experiment in Fig. 3 for comparison), and (3) 200 nm Au nanoparticles embedded in the nano-pillar arrays. As can be seen, integrating the gold nanoparticles with the nano-pillar array yielded a response approximately 50 times higher than the nanoparticle themselves at 1385 cm^{-1} . We also conducted experiments using different concentrations of TAMRA-labeled target probes (50 pM, 100 pM, 250 pM and 500 pM). As can be seen in Fig. 4c, the intensity of the

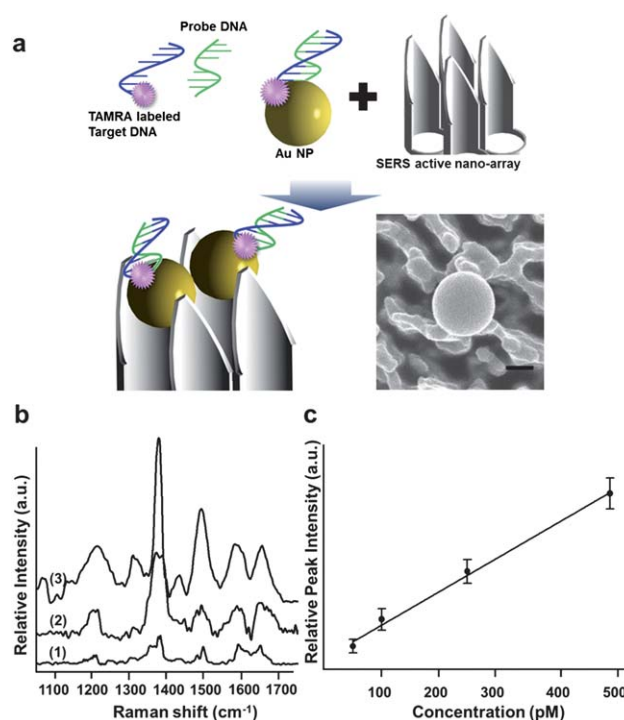


Fig. 4 Integration of substrates with gold nanoparticles enhances SERS response. (a) 200 nm Au nanoparticles were used as SERS enhancers. Hot-spot formation is achieved by spreading the Au nanoparticles onto the type I nano-pillar substrate and a corresponding SEM image (scale bar represents 100 nm). (b) SERS spectra of the TAMRA-labeled DENV-2a for: (1) the Au nanoparticles after settling on a plain surface, (2) the Ag nano-pillar substrate without nanoparticles, and (3) the combined Au nanoparticles and Ag nano-pillar substrate. The concentration of the target DNA in the hybridization reaction was 30 nM. (c) Relative peak intensity of the SERS signal plot at 1385 cm^{-1} (correlation coefficient: $R = 0.987$) corresponding to different initial solution phase concentrations: (1) 50 pM, (2) 100 pM, (3) 250 pM, and (4) 500 pM.

peak at 1385 cm^{-1} increases linearly with the concentration over this range, suggesting the linear trend in the small concentration range can be used for quantitative analysis as well.

Materials and methods

Additional details on the fabrication of the nanostructured arrays

All fabrication steps are described above and summarized in Table 1. Here we provide a few additional details to the reader relevant to being able to repeat these experiments but not to the scientific outcomes. In all cases, AAO membranes (Whatman Anodisc, 60 μm thick, 200 nm diameter pores) were fixed onto a silicon wafer substrate using Kapton® tape and the chuck angle altered from 30° to 60° . Metals (gold and silver) were deposited using a CVC SC4500 (CVC Inc., NY). After the metal deposition, the membranes were detached from the silicon substrate and were immersed in a 3.0 M NaOH solution for 10 min to fully dissolve the AAO sacrificial templates. Following this, the metal nanostructure films were dipped in 30 μM 3-mercaptopropyl-trimethoxysilane (MPTMS) solution for

2 hours which assists the metal film in adhering to the PDMS. After 2 hours the MPTMS solution was replaced with deionized (DI) water and a piece of polymerized PDMS was introduced. The DI water was then gently extracted using a micropipette and the thin metal film was allowed to settle onto the top of the PDMS. The final device was dried in an oven at 80 °C for 1 hour.

Raman measurements

Raman signatures were measured using a Renishaw inVia Raman spectrometer (Renishaw, UK) coupled to a Leica microscope with a 785 nm laser (spectral resolution of approximately 0.1 cm⁻¹). A 50× (NA = 0.75) objective lens was used to focus the laser beam onto the sample surface and the scattered signal was collected by a Peltier cooled CCD detector. Wavenumbers ranging from 1000 cm⁻¹ to 1800 cm⁻¹ were examined here. Raman signals were obtained from at least three different spots on each nanostructured surface.

Sample preparation

Dengue virus serotype 2 (DENV-2) was chosen as the target analyte and purchased from Operon Biotechnologies (Huntsville, AL). The target probe of DENV-2a was modified with TAMRA dye and a thiol-modifier containing C3 S-S functionality. The titrations of TAMRA-labeled target probes were prepared by diluting the proper amount of DNA in a 10 mM PBS buffer solution (0.6 M NaCl, pH 7.4). The 200 nm diameter gold nanoparticles were purchased from Nanocs (New York, NY).

Conclusions

In this work, we have demonstrated a new high throughput technique for creating large area, flexible SERS-active substrates, which we refer to as shadow mask assisted evaporation (SMAE). By controlling the evaporation parameters (incident angle, rotation, and deposition rate) we demonstrated that numerous different topographies can be obtained. We characterized each of these topographies demonstrating that a nano-triangular tip has the largest Raman enhancement and nano-pillar tip has the best repeatability. Integration of these substrates with gold nanoparticles yielded enhanced plasmonic hotspot and resulting in a 50 fold improvement over just the nanoparticles themselves.

Acknowledgements

This work was partially supported by the National Institutes of Health-National Institute of Biomedical Imaging and Bioengineering (NIH-NIBIB) under grant number R21EB007031 and the Nanobiotechnology Center (NBTC), an STC Program of the National Science Foundation under Agreement No. ECS-9876771. Device fabrication for this work was performed in part at the Cornell Nanoscale Facility (CNF), a member of the National Nanotechnology Infrastructure Network, which is supported by the National Science Foundation.

References

- 1 K. Kneipp, H. Kneipp, I. Itzkan, R. R. Dasari and M. S. Feld, *Chem. Rev.*, 1999, **99**, 2957–2976.
- 2 Y. S. Huh, A. J. Chung and D. Erickson, *Microfluid. Nanofluid.*, 2009, **6**, 285–297.
- 3 K. Kneipp, Y. Wang, H. Kneipp, L. T. Perelman, I. Itzkan, R. Dasari and M. S. Feld, *Phys. Rev. Lett.*, 1997, **78**, 1667–1670.
- 4 H.-W. Cheng, S.-Y. Huan, H.-L. Wu, G.-L. Shen and R.-Q. Yu, *Anal. Chem.*, 2009, **81**, 9902–9912.
- 5 T. Kang, S. M. Yoo, I. Yoon, S. Y. Lee and B. Kim, *Nano Lett.*, 2010, **10**, 1189–1193.
- 6 A. Barhoumi, D. Zhang, F. Tam and N. J. Halas, *J. Am. Chem. Soc.*, 2008, **130**, 5523–5529.
- 7 R. M. Li, M. Z. Si, Y. P. Kang, X. F. Zi, Z. Q. Liu and D. Q. Zhang, *J. Colloid Interface Sci.*, 2010, **343**, 52–57.
- 8 Y. Wang, M. Becker, L. Wang, J. Liu, R. Scholz, J. Peng, U. Gösele, S. Christiansen, D. H. Kim and M. Steinhart, *Nano Lett.*, 2009, **9**, 2384–2389.
- 9 J. M. Oran, R. J. Hinde, N. A. Hatab, S. T. Retterer and M. J. Sepaniak, *J. Raman Spectrosc.*, 2008, **39**, 1811–1820.
- 10 D. A. Stuart, J. M. Yuen, N. Shah, O. Lyandres, C. R. Yonzon, M. R. Glucksberg, J. T. Walsh and R. P. Van Duyne, *Anal. Chem.*, 2006, **78**, 7211–7215.
- 11 B. Yan, A. Thubagere, W. R. Premasiri, L. D. Ziegler, L. Dal Negro and B. r. M. Reinhard, *ACS Nano*, 2009, **3**, 1190–1202.
- 12 Y. C. Cao, R. Jin and C. A. Mirkin, *Science*, 2002, **297**, 1536–1540.
- 13 L. Gunnarsson, E. J. Bjerneld, H. Xu, S. Petronis, B. Kasemo and M. Kall, *Appl. Phys. Lett.*, 2001, **78**, 802–804.
- 14 Q. Yu, P. Guan, D. Qin, G. Golden and P. M. Wallace, *Nano Lett.*, 2008, **8**, 1923–1928.
- 15 E. J. Smythe, M. D. Dickey, J. Bao, G. M. Whitesides and F. Capasso, *Nano Lett.*, 2009, **9**, 1132–1138.
- 16 X. Deng, G. B. Braun, S. Liu, P. F. Sciortino, B. Koefer, T. Tomblor and M. Moskovits, *Nano Lett.*, 2010, **10**, 1780–1786.
- 17 M. G. Banaea and K. B. Crozier, *Opt. Lett.*, 2010, **35**, 760–762.
- 18 J. Li, D. Stein, C. McMullan, D. Branton, M. J. Aziz and J. A. Golovchenko, *Nature*, 2001, **412**, 166–169.
- 19 B. D. Gates, Q. Xu, M. Stewart, D. Ryan, C. G. Willson and G. M. Whitesides, *Chem. Rev.*, 2005, **105**, 1171–1196.
- 20 Y.-L. Loo, R. L. Willett, K. W. Baldwin and J. A. Rogers, *J. Am. Chem. Soc.*, 2002, **124**, 7654–7655.
- 21 X. Zhang, J. Zhao, A. V. Whitney, J. W. Elam and R. P. Van Duyne, *J. Am. Chem. Soc.*, 2006, **128**, 10304–10309.
- 22 K. R. Strehle, D. Cialla, P. Rosch, T. Henkel, M. Kohler and J. Popp, *Anal. Chem.*, 2007, **79**, 1542–1547.
- 23 R. G. Freeman, K. C. Grabar, K. J. Allison, R. M. Bright, J. A. Davis, A. P. Guthrie, M. B. Hommer, M. A. Jackson, P. C. Smith, D. G. Walter and M. J. Natan, *Science*, 1995, **267**, 1629–1632.
- 24 H. Wang, C. S. Levin and N. J. Halas, *J. Am. Chem. Soc.*, 2005, **127**, 14992–14993.
- 25 A. Jamshidi, S. L. Neale, K. Yu, P. J. Pauzauskie, P. J. Schuck, J. K. Valley, H.-Y. Hsu, A. T. Ohta and M. C. Wu, *Nano Lett.*, 2009, **9**, 2921–2925.
- 26 L. Y. Wu, B. M. Ross, S. Hong and L. P. Lee, *Small*, 2010, **6**, 503–507.
- 27 C. X. Wang, W. D. Ruan, N. Ji, W. Ji, S. Lv, C. Zhao and B. Zhao, *J. Phys. Chem. C*, 2010, **114**, 2886–2890.
- 28 J. C. Hulteen, M. A. Young and R. P. Van Duyne, *Langmuir*, 2006, **22**, 10354–10364.
- 29 L. A. Dick, A. D. McFarland, C. L. Haynes and R. P. Van Duyne, *J. Phys. Chem. B*, 2001, **106**, 853–860.
- 30 Y. Choi, S. Hong and L. P. Lee, *Nano Lett.*, 2009, **9**, 3726–3731.
- 31 A. Tao, F. Kim, C. Hess, J. Goldberger, R. He, Y. Sun, Y. Xia and P. Yang, *Nano Lett.*, 2003, **3**, 1229–1233.
- 32 S. J. Lee, A. R. Morrill and M. Moskovits, *J. Am. Chem. Soc.*, 2006, **128**, 2200–2201.
- 33 Y. S. Huh and D. Erickson, *Biosens. Bioelectron.*, 2010, **25**, 1240–1243.
- 34 N. Pazos-Perez, S. Barbosa, L. Rodriguez-Lorenzo, P. Aldeanueva-Potel, J. Perez-Juste, I. Pastoriza-Santos, R. A. Alvarez-Puebla and L. M. Liz-Marzan, *J. Phys. Chem. Lett.*, 2010, **1**, 24–27.
- 35 N. C. Linn, C. H. Sun, A. Arya, P. Jiang and B. Jiang, *Nanotechnology*, 2009, **20**, 225303.

-
- 36 S. Rao, M. J. Huttunen, J. M. Kontio, J. Makitalo, M. R. Viljanen, J. Simonen, M. Kauranen and D. Petrov, *Opt. Express*, 2010, **18**, 23790–23795.
- 37 Y. S. Huh, A. J. Chung, B. Cordovez and D. Erickson, *Lab Chip*, 2009, **9**, 433–439.
- 38 N. J. Halas, *Nano Lett.*, 2010, **10**, 3816–3822.
- 39 W. H. Park and Z. H. Kim, *Nano Lett.*, 2010, **10**, 4040–4048.
- 40 N. H. Kim, S. J. Lee and M. Moskovits, *Nano Lett.*, 2010, **10**, 4181–4185.